Mean-Field Dynamics and Fisher Information in Matter Wave Interferometry

Simon A. Haine*
School of Mathematics and Physics, University of Queensland, Brisbane, Queensland 4072, Australia
(Received 20 December 2015; published 9 June 2016)

There has been considerable recent interest in the mean-field dynamics of various atom-interferometry schemes designed for precision sensing. In the field of quantum metrology, the standard tools for evaluating metrological sensitivity are the classical and quantum Fisher information. In this Letter, we show how these tools can be adapted to evaluate the sensitivity when the behavior is dominated by mean-field dynamics. As an example, we compare the behavior of four recent theoretical proposals for gyroscopes based on matter-wave interference in toroidally trapped geometries. We show that while the quantum Fisher information increases at different rates for the various schemes considered, in all cases it is consistent with the well-known Sagnac phase shift after the matter waves have traversed a closed path. However, we argue that the relevant metric for quantifying interferometric sensitivity is the classical Fisher information, which can vary considerably between the schemes.

DOI: 10.1103/PhysRevLett.116.230404

Introduction.—Quantum devices based on matter-wave interferometry, such as atom interferometers [1], atomic Josephson junctions [2], and superfluid helium quantum interference devices [3] have the potential to provide extremely sensitive measurements of inertial quantities such as rotations, accelerations, and gravitational fields [4–12]. While the principles of matter-wave interferometers are well understood, in practice, characterizing and optimizing interferometry schemes is still challenging, as there are many competing effects that can affect the sensitivity [13–15].

While there have recently been proof-of-principle demonstrations of matter-wave interferometers displaying nontrivial quantum correlations [16–24], to date, all matter-wave interferometers with inertial sensing capabilities have been well described by *mean-field* dynamics, which can be obtained by solving either the single particle Schrödinger equation, or the Gross-Pitaevskii equation (GPE) [25]. For example, there have been several recent proposals for atomic gyroscopes based on interference of Bose condensed atoms (BECs) confined in toroidal geometries, or "ring traps"[26–31]. The analysis of these schemes has largely been concerned with the complex multimode dynamics of the *order-parameter* $\psi(\mathbf{r},t)$, which displays rich mean-field dynamics due to the interatomic interactions.

The field of quantum metrology has developed sophisticated tools for evaluating the sensitivity of measurement devices, such as the quantum Fisher information (QFI) and the classical Fisher information (CFI) [32]. However, such analyses are usually concerned with the development of optimal measurement strategies with exotic quantum states, with the goal of providing measurement sensitivities better than the standard quantum limit [33], and largely ignore the classical effects that dominate matter-wave interferometry, such as maximizing interrogation times and mode matching, with which mean-field analyses are concerned. In this Letter, we demonstrate how to calculate the QFI and CFI from the mean-field dynamics of the system, and demonstrate that this is a useful method of quantifying the sensitivity even in the absence of quantum correlations. We apply this technique to four recently proposed schemes [26–29] concerning matter-wave interferometry in ring traps, and show that this technique is very effective at identifying the advantages and disadvantages of each scheme.

Mean-field dynamics and Fisher information.—The fundamental question when assessing the sensitivity of a matter-wave interferometer is the following: By making measurements on the distribution of particles that have been effected by some classical parameter χ (which may be, for example, a parameter quantifying the magnitude of a rotation, acceleration, or gravitational field), how precisely can χ be estimated? The answer is given by the quantum Cramer-Rao bound [34], which dictates that the smallest resolvable change in χ is $\delta\chi = (1/\sqrt{\mathcal{F}_Q})$ where $\mathcal{F}_Q$ is the QFI, which for pure states is $\mathcal{F}_Q = 4[\langle\dot{\Psi}|\dot{\Psi}\rangle - |\langle\Psi|\dot{\Psi}\rangle|^2]$, where $|\dot{\Psi}\rangle = (\partial/\partial\chi)|\Psi\rangle$ [32,35]. The analysis in [26–29] is largely concerned with the complicated multimode mean-field dynamics of the order parameter $\psi(\mathbf{r},t)$, which is simulated via the GPE [25], from which the mean density distribution can be calculated. The QFI is not normally considered in a mean-field analysis, as these calculations are agnostic about the form of the full quantum state $|\Psi\rangle$. While the order parameter $\psi(\mathbf{r})$ is not usually considered as a quantum object, by assuming that the full N-particle state of the system is uncorrelated, we can use $\psi(\mathbf{r})$ to calculate the QFI. Specifically, we make the reasonable assumption [36] that $|\Psi(t)\rangle = [(\hat{a}^\dagger_\psi(t)]^N/\sqrt{N!})|0\rangle$, where $\hat{a}_\psi(t) = \int_{\mathbf{R}^3}\psi^*(\mathbf{r},t)\hat{\psi}(\mathbf{r})d^3\mathbf{r}$, or equivalently, that the system is represented by a many-body wave function of the form

$\Psi(\mathbf{r}_1, \mathbf{r}_2, \ldots, \mathbf{r}_N) = \psi(\mathbf{r}_1)\psi(\mathbf{r}_2), \ldots, \psi(\mathbf{r}_N)$. Because of the additive nature of QFI for separable systems [35], the QFI becomes $\mathcal{F}_Q = NF_Q$, where

$$F_Q = 4\left[\int_{\mathbf{R}^3} \dot{\psi}^* \dot{\psi} d^3\mathbf{r} - \left|\int_{\mathbf{R}^3} \psi^* \dot{\psi} d^3\mathbf{r}\right|^2\right] \quad (1)$$

is the *single particle* QFI, and $\dot{\psi} = (\partial/\partial\chi)\psi(\mathbf{r}, t)$. The QFI tells us in principle how much information about the parameter χ that the state $|\Psi\rangle$ contains, assuming that we have complete freedom in the choice of measurement. However, in the case of matter-wave interferometry, we are usually limited to making measurements of the spatial distribution of particles, as is the case via optical fluorescence, absorption, or phase-contrast imaging [37], or detection via multichannel arrays such as is common in experiments with metastable helium [38]. Because of the nature of these imaging techniques, only two dimensions of the spatial distribution at a single snapshot in time can be obtained, with the third dimension integrated over [37]. In this case we are restricted to the information that is contained in spatial probability distribution, and the sensitivity is limited to $\Delta\chi = (1/\sqrt{\mathcal{F}_C})$, where $\mathcal{F}_C$ is the CFI. Again, assuming that our many-body quantum state is uncorrelated, we can view the detection of the position of each atom as N uncorrelated events, such that the CFI is simply $\mathcal{F}_C = NF_C$, where

$$F_C = \int_{\mathbf{R}^2} \frac{1}{P(x,y)}\left(\frac{\partial P}{\partial \chi}\right)^2 dxdy, \quad (2)$$

and $P(x, y) = \int |\psi(\mathbf{r}, t)|^2 dz$, where we have chosen the z direction as the imaging axis. The CFI quantifies how precisely we can estimate χ based purely on measurements of the two dimensional position distribution function. By optimizing over all possible measurements it can be shown that $\mathcal{F}_Q \geq \mathcal{F}_C$ [32].

Obviously, by assuming that our state is uncorrelated, as with all mean-field treatments, we are ignoring the effects of any possible quantum correlations between the particles. However, in all matter-wave interferometer inertial sensors so far demonstrated, the atomic sources are well approximated by uncorrelated systems [1]. Additionally, in many of these experiments, the detection efficiency is low, or there are significant sources of loss [13], which has the effect of diminishing the importance of any correlations.

Comparison of matter-wave gyroscopes.—When a matter wave in a rotating frame is split such that it traverses two separate paths enclosing an area A, the components in each path accumulate a phase difference given by the well-known Sagnac effect

$$\phi_S = \frac{2m}{\hbar}\boldsymbol{\Omega} \cdot \mathbf{A}, \quad (3)$$

where m is the mass of the particle, $\mathbf{A} = A\hat{\mathbf{n}}$, where $\hat{\mathbf{n}}$ is the unit vector normal to the enclosed area, and $\boldsymbol{\Omega}$ is the angular velocity [1]. We now turn our attention to the specific case of an interferometric matter-wave gyroscope confined in a ring trap. In particular, we aim to use F_Q and F_C as a tool to compare the recent theoretical proposals [26–29]. Our aim is not to replicate every detail of these proposals, but to demonstrate how F_C and F_Q illuminate important aspects and the advantages and disadvantages of each scheme. As in [26–28], working in cylindrical coordinates $\{r, z, \theta\}$, we assume a trapping potential of the form $V(\mathbf{r}) = \frac{1}{2}m[\omega_z^2 z^2 + \omega_r^2(r - R)^2]$, where R is the radius of the torus and ω_r and ω_z are the radial and axial trapping frequencies. Assuming that the radial and axial confinement is sufficiently tight, we may ignore the dynamics in these directions, in which case the evolution of the order parameter is described by the equation

$$i\hbar\frac{d}{dt}\psi(\theta, t) = \left(\frac{-\hbar^2}{2mR^2}\frac{\partial^2}{\partial\theta^2} + U|\psi|^2 - \Omega\hat{L}_z\right)\psi(\theta, t), \quad (4)$$

where $\hat{L}_z$ is the z component of the angular momentum, and we have assumed that we are working in a frame rotating around the z axis at angular frequency Ω. The goal of the device is to estimate Ω based on measurements of the matter waves. We first restrict ourself to the noninteracting case $U = 0$. In this case, $\hat{L}_z$ commutes with the other terms in the Hamiltonian which allows us to solve for the dynamics of $\psi(\theta, t)$ analytically: $\psi(\theta, t) = \hat{U}_\Omega \hat{U}_{KE}\psi(\theta, 0)$, where $\hat{U}_\Omega = \exp(i\Omega\hat{L}_z t/\hbar)$, and $\hat{U}_{KE} = \exp(it\hbar/2mR^2[\partial^2/\partial\theta^2])$, which allows us to evaluate

$$F_Q(t) = 4t^2 V(\hat{L}_z/\hbar), \quad (5)$$

where the variance may be computed with respect to either the initial state $\psi(\theta, 0)$ or the state at some later time $\psi(\theta, t)$. From this, we see that initial states with a large spread in angular momentum will accumulate QFI more rapidly. To evaluate F_C, we solve for $\psi(\theta, t)$, calculate $P(\theta, t) = |\psi(\theta, t)|^2$ for a range of different values of Ω, and then calculate the derivative in Eq. (2) numerically. We first examine the scheme proposed by Kandes *et al.* [27]. They simulate a Gaussian wave packet (centered at $\theta = 0$, initially at rest in the rotating frame), which is then split into two counterpropagating components with momentum $\pm\hbar k_{\text{kick}}$. The wave packets then traverse the ring in opposite directions, colliding (and passing through each other) on the far side of the ring ($\theta = \pi$), and again back at $\theta = 0$. Figure 1(a) shows $P(\theta, t)$, which displays high-contrast interference fringes as the wave packets pass through one another. The position of these fringes depends on the value of Ω used in the simulation. Figure 1(b) shows $dP(\theta, t)/d\Omega$, generated by performing simulations with slightly different values of Ω. It can be seen that the derivative is negligible

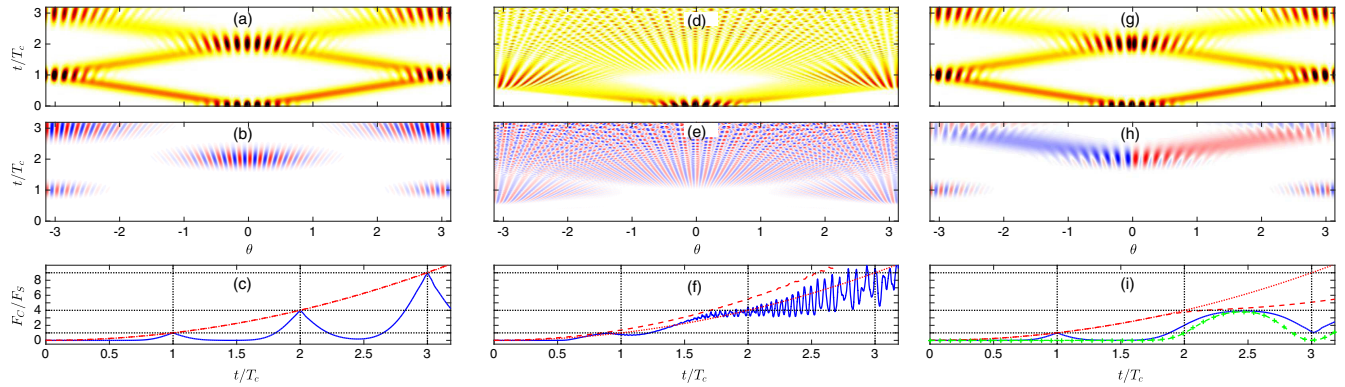

FIG. 1. (a), (d), (g) $P(\theta, t)$ simulated with $\Omega = 0$ (low density, white; high density, dark). (b), (e), (h) $dP(\theta, t)/d\Omega|_{\Omega=0}$ (positive, red; negative, blue; zero, white). (c), (f), (i) F_Q (red dashed line), F_C (blue solid line), F_{LR} [green + symbols, (i) only], and $4t^2R^2k_{\text{kick}}$ (red dotted line). The vertical dotted lines indicate integer multiples of the classical collision time T_c and the horizontal dotted lines indicate n^2F_S, for integer values of n, indicating the number of closed loops the wave packets have traversed. Parameters: For all frames, $\psi(\theta, 0) = \sqrt{2}(\sigma\sqrt{\pi/2})^{-1/2}\exp(-\theta^2/2\sigma^2)\cos(k_{\text{kick}}R\theta)$, $\sigma = 0.5$ rad, $k_{\text{kick}} = 20/R$. (a)–(c) and (g)–(i) $U = 0$; (d)–(f) $U = 0.2\hbar/mR$. In frames (g)–(i), a repulsive delta-function potential was introduced at $\theta = 0$ and $t = T_c$.

except when the wave packets are overlapping. The asymmetric nature of the derivative indicates that small deviations in Ω can be inferred from the spatial position of the fringes. Figure 1(c) shows F_Q and F_C vs time. As expected, F_Q displays quadratic time dependence with prefactor $V(\hat{L}_z/\hbar) \approx R^2k_{\text{kick}}^2$. The CFI is initially zero, but when the wave packets begin to overlap, F_C increases such that $F_C \approx F_Q$. The times at which this occurs is at integer multiples of the classical collision time $T_c = \pi Rm/\hbar k_{\text{kick}}$, at which $F_Q \approx F_S = (2m\pi R^2/\hbar)^2$, where F_S is defined as the QFI of a state where the phase of two components differs by the Sagnac phase shift: $|\Psi\rangle = (1/\sqrt{2})(|\psi_1\rangle + |\psi_2\rangle e^{i\phi_S})$, where ϕ_S is given by Eq. (3), and $\langle\psi_i|\psi_j\rangle = \delta_{ij}$. This quantity represents idealized operation of a matter-wave gyroscope after one closed loop has been traversed. From this analysis, we see that the magnitude of k_{kick} increases the rate at which F_Q accumulates, but it ultimately doesn't affect the value of F_Q after an integer number of closed loops have been traversed. As we are restricted to measurements of the spatial distribution of particles, F_C is the relevant quantity, which is sharply peaked around integer multiples of T_c, indicating that it is crucial to make the measurement at the collision times.

So far these results are not particularly surprising. However, this analysis allows us to deal with more complicated systems where our analytic insight breaks down. One such example is by including a nonlinear interaction $U \neq 0$ in Eq. (4). Figure 1(d) shows an identical simulation to Fig. 1(a), except with $U = 0.2\hbar/mR$. The wave packets now disperse much more rapidly until they become larger than the circumference of the ring, and the notion of a classical collision time and Sagnac phase shift becomes ill defined. However, our Fisher information analysis sheds some light on the usefulness of this device [Fig. 1(f)]. F_Q increases more rapidly than the noninteracting case, and F_C is no longer sharply peaked around integer multiples of T_c. Although F_C is less than F_Q for all time, it is also significantly greater than zero, and can be greater than F_S, indicating the existence of a method of processing the information contained in $P(\theta)$ in order to extract Ω, even when the concept of the Sagnac phase shift Eq. (3) become irrelevant due to different momentum components traversing different number of closed loops. Kandes *et al.* [27] provide a method of extracting the phase shift based on analyzing different frequency components of the density distribution, but this method assumes perfect signal-to-noise ratio and cannot make predictions on the metrological sensitivity of the device, which our analysis does.

In both of the above calculations, the rotational information is contained in the position of the interferences fringes in the density. This would require high-resolution spatial imagining, which could be challenging if the wavelength of the fringes becomes small. Helm *et al.* [28] model a similar scheme, except that each wave packet partially reflects off a sharp delta-function "barrier" at $\theta = 0$, acting as a matter-wave beam splitter to convert the phase information into population information of the two counterpropagating wave packets. The height of the barrier is tuned such that the wave packets undergo 50% quantum reflection, and the clockwise and counterclockwise propagating components can interfere. Figure 1(g) shows that the system behaves identically to that of Kandes *et al.* until the wave packets encounter the barrier at $t \approx 2T_c$, after which time the relative populations of the counterpropagating wave packets depends on Ω. This is reflected in F_C, which displays a plateau of $F_C \approx 4F_S$ after $2T_c$ until the wave packets collide again, creating ambiguity in the population of each wave packet. If our imaging system cannot fully resolve the details of the density distribution, but can distinguish between the right-going and left-going matter-wave components, then the appropriate CFI is $F_{LR} = \sum_{j=L,R} P_j^{-1}(\partial P_j/\partial\Omega)^2$,

where $P_L = \int_{-\pi}^{0} P(\theta)d\theta$, $P_R = \int_{0}^{\pi} P(\theta)d\theta$ are the components of the matter wave on the left and right of the barrier respectively. Figure 1(i) shows that F_{LR} is comparable to F_C, indicating that a measurement of the fraction of atoms on either side of the barrier is sufficient to extract the rotation information from the system. We note that although Helm *et al.* focus on the soliton regime for their simulations, we see that by simply using noninteracting wave packets, F_{LR} approaches F_S, indicating that this approach is sufficient to observe the full information from the Sagnac effect, without the need for operating in the soliton regime.

Halkyard *et al.* [26] consider a different approach, where the matter wave is initially in the ground state of the potential, which uniformly fills the ring. A coupling pulse is then used to coherently transfer 50% of the population to a different spin state while also transferring orbital angular momentum $\hbar\ell$ to this component. The two components remain spatially overlapped but accumulate a phase difference at a rate $\Delta\phi = 2\ell\Omega t$, which is then converted into either a population difference or density modulation between the two components via Ramsey interferometry. For simplicity, and as it highlights the important features of the scheme, we will initially consider only a single spin state, consisting of an equal superposition of $\hat{L}_z$ eigenstates with eigenvalues $\pm\hbar\ell$: $\psi(\theta,0) = (1/\sqrt{4\pi})(e^{i\ell\theta} + e^{-i\ell\theta})$. In this case we have an exact expression for the variance of $\hat{L}_z$: $V(\hat{L}_z) = \hbar^2\ell^2$, and $F_Q = 4\ell^2 t^2$. Furthermore, it is trivial to solve for $\psi(\theta,t)$, which allows us to calculate the probability distribution $P(\theta,t) = 1 + \cos[2\ell(\theta + \Omega t)]$, from which we can calculate the $F_C = 4\ell^2 t^2 = F_Q$, indicating that a measurement of the density saturates the Cramer-Rao bound for all time. That is, as the wave packets are spatially overlapping for all times, information about the phase due to angular rotation can be observed in the density as persistent interference fringes.

A common technique for overcoming the requirement for high spatial resolution is to use an additional degree of freedom such as the atomic spin [39]. If our two spin states are $|+1\rangle$ and $|-1\rangle$, then a general single particle state is $|\psi\rangle = \psi_{+1}(\mathbf{r})|+1\rangle + \psi_{-1}(\mathbf{r})|-1\rangle$. If our N-particle state is simply an uncorrelated product state, then $\mathcal{F}_Q = NF_Q$ where $F_Q = 4(\langle\dot{\psi}|\dot{\psi}\rangle - |\langle\dot{\psi}|\psi\rangle|^2)$. By coherently coupling these two spin states via either a microwave or Raman transition, the phase information can be converted into population information, such that a measurement of the total number of particles in spin state, rather than the spatial distribution, is all that is required. If we restrict ourselves to measurements of the population of each spin state, then $F_C = \sum_{j=+1,-1} P_j^{-1}(dP_j/d\Omega)^2$, where $P_j = |\langle j|\psi\rangle|^2$ is the probability of finding each particle in the spin state $|j\rangle$. We now return to the example of Halkyard *et al.*, who prepare an initial state such that $\psi_{\pm1}(\theta,0) = (1/2\sqrt{\pi})e^{\pm i\ell\theta}$, which after time T evolves to $\psi_{\pm1}(\theta,T) = (1/2\sqrt{\pi})e^{\pm i\ell\theta}e^{\pm i\ell\Omega T}$. The two spin components are then coupled via a coherent Raman transition which transfers 2ℓ units of orbital angular momentum, such that at the final time t_f the state is $\psi_{\pm1}(\theta,t_f) = (1/\sqrt{2})[\psi_{\pm1}(\theta,T) - i\psi_{\mp1}(\theta,T)e^{\pm 2i\ell\theta}]$. From this expression its simple to calculate the Fisher information and arrive at $F_Q = F_C = 4\ell^2T^2$.

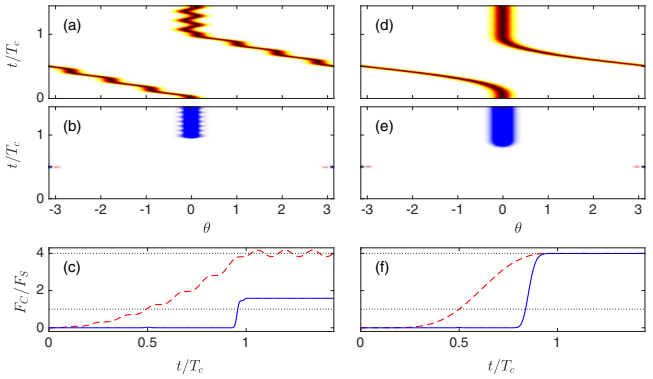

FIG. 2. (a), (d) $|\psi_{+1}(\theta,t)|^2$ (low density, white; high density, dark). $|\psi_{-1}(\theta,t)|^2$ is identical to $|\psi_{+1}(\theta,t)|^2$ except reflected around $\theta = 0$. (b), (e) $\partial J_z(\theta,t)/\partial\Omega$, where $J_z = \frac{1}{2}(|\psi_{+1}(\theta,t_f)|^2 - |\psi_{-1}(\theta,t_f)|^2)$ (positive, red; negative, blue; zero, white). (c), (f) F_Q (red dashed line), F_C (blue solid line). Each component was initially in the ground state of a spin dependent, harmonic trapping potential $V_{\pm}(\theta) = \frac{1}{2}m\omega_\theta^2 R^2(\theta - \theta_0)^2$. In (a), (b), (c), the trap minimum moved with constant velocity: $\theta_0(t) = \mp 2\pi t/T_c$, and in (d), (e), (f), the trap minimum moved with a sinusoidal velocity profile: $\theta_0 = 2\pi t/T_c - \sin(2\pi t/T_c)$. Parameters: $R = 5\sqrt{\hbar/m\omega_\theta}$, $T_c = 5\omega_\theta^{-1}$.

Finally, we consider the case of Stevenson *et al.* [29], who depart from the notion of freely propagating matter waves, and consider two spin components $|+1\rangle$ and $|-1\rangle$, where the trapping potential for each component can be manipulated independently. The two spin components are transported around a closed loop in opposite directions via a time-dependent trapping potential, and then recombined via a microwave coupling pulse at time T such that the state of the system at the final time t_f is $\psi_{\pm1}(\theta,t_f) = (1/\sqrt{2})[\psi_{\pm1}(\theta,T) - i\psi_{\mp1}(\theta,T)]$. Figure 2 shows the density distribution for one component, $\partial J_z(\theta,t)/\partial\Omega$, where $J_z = \frac{1}{2}[|\psi_{+1}(\theta,t_f)|^2 - |\psi_{-1}(\theta,t_f)|^2]$, and F_C and F_Q for two different cases. In the first case, the minimum of the harmonic trapping potential for each component moves from $\theta = 0$ to $\theta = \pi$ with constant velocity, which creates a centre of mass "sloshing" excitation, which inhibits the overlap of the two components such that F_C is significantly less than F_Q. In the second case, the potential minimum moves with a sinusoidal velocity profile which creates far less mechanical excitation, and $F_C \approx F_Q$.

Conclusion.—We have shown that both the CFI and QFI are useful tools for evaluating the mean-field dynamical aspects of matter-wave interferometry. The quantum Fisher information automatically accounts for any phase information, even in cases where a simple notion of a phase shift

may be ill defined, or when there is no simple analytic expression for the phase evolution. The CFI automatically accounts for any issues of imperfect wave-packet overlap, and is the appropriate metric for the metrological information that can be extracted from measurements of the density distribution. This theoretical technique may be useful for analyzing the sensitivity of devices where the dynamics is dominated by mean-field effects, such as atomic Josepheson junctions, or superfluid helium quantum interference devices.

The author would like to acknowledge useful discussions with Michael Bromley, Robin Stevenson, Sam Nolan, Stuart Szigeti, and Matthew Davis. The numerical simulations were performed with XMDS2 [40]. This work was supported by Australian Research Council (ARC) Discovery Project No. DE130100575.

*simon.a.haine@gmail.com

[1] A. D. Cronin, J. Schmiedmayer, and D. E. Pritchard, Rev. Mod. Phys. **81**, 1051 (2009).
[2] C. Ryu, P. W. Blackburn, A. A. Blinova, and M. G. Boshier, Phys. Rev. Lett. **111**, 205301 (2013).
[3] E. Varoquaux, Rev. Mod. Phys. **87**, 803 (2015).
[4] F. Riehle, T. Kisters, A. Witte, J. Helmcke, and C. J. Bordé, Phys. Rev. Lett. **67**, 177 (1991).
[5] T. L. Gustavson, P. Bouyer, and M. A. Kasevich, Phys. Rev. Lett. **78**, 2046 (1997).
[6] A. Lenef, T. D. Hammond, E. T. Smith, M. S. Chapman, R. A. Rubenstein, and D. E. Pritchard, Phys. Rev. Lett. **78**, 760 (1997).
[7] T. L. Gustavson, A. Landragin, and M. A. Kasevich, Classical Quantum Gravity **17**, 2385 (2000).
[8] D. S. Durfee, Y. K. Shaham, and M. A. Kasevich, Phys. Rev. Lett. **97**, 240801 (2006).
[9] B. Canuel, F. Leduc, D. Holleville, A. Gauguet, J. Fils, A. Virdis, A. Clairon, N. Dimarcq, C. J. Bordé, A. Landragin, and P. Bouyer, Phys. Rev. Lett. **97**, 010402 (2006).
[10] S. Wu, E. Su, and M. Prentiss, Phys. Rev. Lett. **99**, 173201 (2007).
[11] J. K. Stockton, K. Takase, and M. A. Kasevich, Phys. Rev. Lett. **107**, 133001 (2011).
[12] S. M. Dickerson, J. M. Hogan, A. Sugarbaker, D. M. S. Johnson, and M. A. Kasevich, Phys. Rev. Lett. **111**, 083001 (2013).
[13] S. S. Szigeti, J. E. Debs, J. J. Hope, N. P. Robins, and J. D. Close, New J. Phys. **14**, 023009 (2012).
[14] K. S. Hardman, C. C. N. Kuhn, G. D. McDonald, J. E. Debs, S. Bennetts, J. D. Close, and N. P. Robins, Phys. Rev. A **89**, 023626 (2014).
[15] G. D. McDonald, C. C. N. Kuhn, K. S. Hardman, S. Bennetts, P. J. Everitt, P. A. Altin, J. E. Debs, J. D. Close, and N. P. Robins, Phys. Rev. Lett. **113**, 013002 (2014).
[16] J. Hald, J. L. Sørensen, C. Schori, and E. S. Polzik, Phys. Rev. Lett. **83**, 1319 (1999).
[17] A. Kuzmich, L. Mandel, and N. P. Bigelow, Phys. Rev. Lett. **85**, 1594 (2000).
[18] C. Gross, T. Zibold, E. Nicklas, J. Estève, and M. K. Oberthaler, Nature (London) **464**, 1165 (2010).
[19] M. F. Riedel, P. Böhi, Y. Li, T. W. Hänsch, A. Sinatra, and P. Treutlein, Nature (London) **464**, 1170 (2010).
[20] I. D. Leroux, M. H. Schleier-Smith, and V. Vuletić, Phys. Rev. Lett. **104**, 073602 (2010).
[21] B. Lücke, M. Scherer, J. Kruse, L. Pezzé, F. Deuretzbacher, P. Hyllus, O. Topic, J. Peise, W. Ertmer, J. Arlt, L. Santos, A. Smerzi, and C. Klempt, Science **334**, 773 (2011).
[22] Z. Chen, J. G. Bohnet, S. R. Sankar, J. Dai, and J. K. Thompson, Phys. Rev. Lett. **106**, 133601 (2011).
[23] R. J. Sewell, M. Koschorreck, M. Napolitano, B. Dubost, N. Behbood, and M. W. Mitchell, Phys. Rev. Lett. **109**, 253605 (2012).
[24] C. D. Hamley, C. S. Gerving, T. M. Hoang, E. M. Bookjans, and M. S. Chapman, Nat. Phys. **8**, 305 (2012).
[25] F. Dalfovo, S. Giorgini, L. P. Pitaevskii, and S. Stringari, Rev. Mod. Phys. **71**, 463 (1999).
[26] P. L. Halkyard, M. P. A. Jones, and S. A. Gardiner, Phys. Rev. A **81**, 061602 (2010).
[27] M. C. Kandes, R. Carretero-Gonzalez, and M. W. J. Bromley, arXiv:1306.1308.
[28] J. L. Helm, S. L. Cornish, and S. A. Gardiner, Phys. Rev. Lett. **114**, 134101 (2015).
[29] R. Stevenson, M. R. Hush, T. Bishop, I. Lesanovsky, and T. Fernholz, Phys. Rev. Lett. **115**, 163001 (2015).
[30] S. P. Nolan, J. Sabbatini, M. W. J. Bromley, M. J. Davis, and S. A. Haine, Phys. Rev. A **93**, 023616 (2016).
[31] T. A. Bell, J. A. P. Glidden, L. Humbert, M. W. J. Bromley, S. A. Haine, M. J. Davis, T. W. Neely, M. A. Baker, and H. Rubinsztein-Dunlop, New J. Phys. **18**, 035003 (2016).
[32] G. Tóth and I. Apellaniz, J. Phys. A **47**, 424006 (2014).
[33] D. J. Wineland, J. J. Bollinger, W. M. Itano, F. L. Moore, and D. J. Heinzen, Phys. Rev. A **46**, R6797 (1992).
[34] S. L. Braunstein and C. M. Caves, Phys. Rev. Lett. **72**, 3439 (1994).
[35] R. Demkowicz-Dobrzański, M. Jarzyna, and J. Kołodyński, Prog. Opt. **60**, 345 (2015).
[36] A. J. Leggett, Rev. Mod. Phys. **73**, 307 (2001).
[37] W. Ketterle, D. S. Durfee, and D. M. Stamper-Kurn, Making, Probing and Understanding Bose-Einstein Condensates, in *Proceedings of the International School of Physics "Enrico Fermi," Course CXL*, edited by M. Inguscio, S. Stringari, and C. Wieman (IOS Press, Amsterdam, 1999), p. 67.
[38] W. Vassen, C. Cohen-Tannoudji, M. Leduc, D. Boiron, C. I. Westbrook, A. Truscott, K. Baldwin, G. Birkl, P. Cancio, and M. Trippenbach, Rev. Mod. Phys. **84**, 175 (2012).
[39] C. Borde, Phys. Lett. A **140**, 10 (1989).
[40] G. R. Dennis, J. J. Hope, and M. T. Johnsson, Comput. Phys. Commun. **184**, 201 (2013).